Boron/Nitrogen Flame Retardant Additives Cross-linked Cellulose Nanofibril/Montmorillonite Aerogels towards Super Low Flammability and Improved Mechanical Properties

Liang Wang [1*], Miguel Sánchez-Soto [2], Jie Fan [1], Zhao-Peng Xia [1] and Yong Liu [1*]

1 School of Textiles, Key Laboratory of Advanced Textiles Composites of Ministry of Education, Tianjin Polytechnic University, Binshui West Road 399, Xiqing Distinct, 300387,Tianjin, China.

2 Centre Catalá del Plástic, Universitat Politécnica de Catalunya, Barcelona Tech., Colom 114, 08222 Terrassa, Spain.

***** Correspondence: Liang Wang, liangwang@tjpu.edu.cn; Yong Liu, liuyong@tjpu.edu.cn.

Tel: +86-22-83955298. Binshui West Road 399, Xiqing Distinct, 300387,Tianjin, China.

Abstract: Low-flammability freeze-dried cellulose nanofibril (CNF)/sodium montmorillonite (MMT) aerogels with improved mechanical properties were fabricated via a facile cross-linking of boric acid (BA) and melamine-formaldehyde (MF) resins. Scanning electron microscopy analysis showed that BA cross-linking reduced the interspacing of layered CNF/MMT aerogels whereas introduction of MF formed polymeric fibrils that connected the layers. These changes on microstructures resulted in the improvement on compressive mechanical properties of the cross-linked aerogels. Moreover, the boron (B)/nitrogen (N) containing flame retardant cross-linkers greatly increased the limiting oxygen index values that could reach 85% and leveled the UL-94 rating from no rating to V-0. Cone calorimetric results suggested that BA and MF induced a synergistic effect on the flame retardant properties of the CNF/MMT aerogels. However, the thermal conductivity was little affected because pore structure and size was not substantially modified. This simple approach fabricated highly flame-resistant and mechanically strong CNF based aerogels that could be used in various engineering fields.

Keywords: Foams, Cellulose Nanofibril, Flame Retardancy, Mechanical Testing.

Running title: Low-flammability green foam

1. Introduction

Aerogel are a family of ultralight solid materials with excellent physical and chemical properties, such as high porosity, large specific surface area and low thermal conductivity (1). Since their discovery by Kistler in 1931 (2, 3), aerogels have been receiving extensive attention due to their potential applications in thermal insulation (4), catalyst carrier (5), waste water treatment (6), tissue engineering (7), energy storage (8), flexible device (9) etc.

Recently foam-like aerogels prepared from renewable resources have been subject of considerable interest as promising bio-based alternatives for petroleum-derived foams. A range of biopolymers have been utilized to prepare green aerogels, such as casein (10), alginate (11), pectin (12, 13) xanthan gum (14) and starch (15), etc.. Cellulose is the most abundant renewable polymer on earth. In particular, cellulose nanofibrils (CNFs) isolated from plant, have excellent mechanical properties and high aspect ratio (16, 17). Ikkala (18) and Berglund (19) pioneered CNF aerogels from CNF gels that were composed of entangled nanofibers. CNFs are typically dispersed in aqueous suspensions prior to preparation of aerogels. A strong network structure is formed between CNFs via hydrogen bonding in the aerogels. Moreover, CNFs maintain the crystalline structure of cellulose I endowing a high thermal stability of CNF aerogels (20, 21). Bio-based CNF aerogel have become a focus of the past decade of research. However, one of the most important issues that need to be addressed for the wide use of CNFs aerogels is the improvement of their mechanical properties. Strategies such as polymer blending (22-24) or matrix cross-linking (25-27) have been applied, providing mechanically strong aerogels.

Flame resistance is another important property expected for porous CNF aerogels that are highly flammable in nature. Inorganic phases have been introduced by in-situ formation (28-30), physical blending (31-32) or layer-by-layer on the surface (33) to form a char that acted like a barrier preventing burning of the underlying substrate. A synergistic flame retardant effect was achieved via incorporating clay and flame retardant agents (FRAs) (34) or phosphorylation of CNF (35). However, these strategies do not have significant contribution on the mechanical properties of aerogels due to primary weak Van deer Far force between the FRAs or inorganic nanofillers and CNFs. Therefore, it is a challenge to realize cross-linking between FRA and cellulose

matrix to obtain aerogels that show a combination of excellent mechanical performance and fire resistant properties.

A few works were reported to achieve dual modifications on polymeric aerogels. Wicklein et al prepared borate cross-linked CNF aerogels that showed improved fire resistance and mechanical properties (36). Guo et al. used N-methylol dimethylphosphonopropionamide to cross-link CNF and fabricated aerogels displayed high flexibility and self-extinguishing behavior (37). However, incorporation of single FRA could not significantly depress the flammability of CNF aerogels, which still displayed low limiting oxygen index values after flame retardant modification. Synergistic flame retardant effect between nitrogen (N)/phosphor (P) or N/boron (B) containing FRAs can be achieved by adequately combining them. This strategy has been widely used in the flame retardant modification of polymeric products (38). To the best of our knowledge, N/B synergistic effect on the flame retardancy and mechanical properties of CNF based aerogels has not been yet studied.

In this work, CNF/MMT aerogels were prepared via a freeze-drying method. Boric acid and MF resins were added as B-containing and N-containing FRAs respectively. CNF were cross-linked by MF and boric acid to form network structures. The morphologies, compressive mechanical properties, thermal stability as well as flammability of prepared aerogels were investigated.

2. Materials and Methods

2.1 Materials

TEMPO-oxidized cellulose nanofibrils (CNFs, diameter: 4-10 nm, length: 1-3 μm) were bought from Guilin Qihong technology co., Ltd (Guilin, China). Sodium montmorillonite (Na^+-MMT, PGW grade, produced by Nanocor Inc.) with a cation exchange capacity of 145meq/100g was purchased from Beijing Yiwei Specialization Technology Co. Ltd. Melamine-formaldehyde resins (MF, permute XR-9181) were supplied by Starr Paint Co., Ltd (Suzhou, China). Boric acid (BA) powder was provided by Tianjin Jizhun Chemical Reagent Co., Ltd (Tianjin, China). Hydrochloric acid with purity of 30% was acquired from Tianjin Sailboat Chemical Reagent Technology Co., Ltd. All chemicals were used without further purification.

2.2 Preparation of CNF/MMT Composite Aerogels

To prepare CNF/MMT precursor suspensions, 2.25 g dry CNFs were first dispersed in 100 mL deionized (DI) water through mechanical stirring at 1200 rmp for 1 hours. Meanwhile, 0.25 g MMT were dispersed in 50 mL DI water via homomixer (ART-D9, Germany) at 20 000 rmp for 10 minutes. Finally, 50 mL of 0.5 % MMT suspensions were mixed with 100 mL of 2.25 % CNF suspensions via mechanical stirring for 1 hour followed by sonication for 20 minutes. The obtained homogenous precursors were then poured into desired molds and frozen in an ethanol/liquid nitrogen bath (-116 ^{o}C) for 30 minutes. Finally, the frozen gels were freeze-dried using a lyophilizer (Scientz-10N, China) under a vacuum of 1 Pa and a condenser temperature of -55 ^{o}C for 72 hours.

2.3 Preparation of cross-linked CNF/MMT Composite Aerogels

To prepare a BA cross-linked CNF/MMT aerogel, the CNF/MMT suspensions previously described were first prepared. Then variable amounts of BA powder were mixed mechanically to obtain cross-linked gels. This reaction was carried out at room temperature for 2 h. Finally, the gels were frozen and freeze dried.

The N/B FRA modified CNF/MMT composite aerogels were prepared following the scheme shown in Figure 1. MF resin (2.25 g) was added to the aforementioned prepared CNF/MMT/BA suspension and dispersed evenly through mechanical stirring for 1 h. Then the pH was adjusted to pH=4 via dropwise addition of hydrochloric acid. The resulting mixtures were frozen and lyophilized in the same manner. Finally, the aerogels containing MF were placed in an oven at 80 ^{o}C for 8 h to achieve cross-linking. The compositions of the aerogel were noted as each component following by its corresponding weight ratio to 100 mL of DI water respectively. The composite C1.5M0.17 was used as a control sample.

Figure 1. Scheme illustrating the procedure used to synthesize N/B FRAs modified CNF/MMT composite aerogels.

2.4 Characterizations

A Bolin rheometer was used to determine the viscosity and shear stress of precursor suspensions for preparing aerogels at ambient temperature (25 ^{o}C) with a shear rate range from 0.1 to 450 1/s.

Infrared spectra were recorded on a Nicolet iS50 Fourier infrared spectrophotometer in the attenuated total reflectance mode (FTIR-ATR, Thermo Fisher, USA) and the corresponding spectral were based on 30 scans with a resolution of 0.1 cm^{-1} across a wavenumber interval between 4000 and 400 cm^{-1}.

The X-ray photoelectron spectroscopy (XPS) spectra were collected using monochromatic Al K-alpha X-ray source (Thermo Fisher, USA) operated at 150 W. An analyzer pass energy of 200 eV for acquiring wide spectra and a pass energy of 50 eV for individual photoelectron lines were used.

The morphologies of aerogels were charaterized by a scanning electron microscope (SEM, Hitachi-TM3030, Japan) at an acceleration voltage of 15 kV. Prior to the observation, specimens were cyro-fractured and sputter coated with a conductive gold layer.

The apparent densities (ρ_{app}) of aerogels were calculated by the division of mass to volume of cylinder samples. Five specimens were taken for each composition.

The solid densities (ρ_s) of aerogels were theoretically calculated according to the equation 1.

$$\boldsymbol{\rho_s} = \frac{\mathbf{1}}{\sum_{n}^{i=1} \boldsymbol{W_i}/_{\boldsymbol{\rho_i}}} \qquad \text{(eq.1)}$$

Where, W_i and ρ_i are the mass fraction and densities of each components, respectively. The densities of CNFs (1.46 g/cm^3), MMT (2.6 g/cm^3), MF (1.57 g/cm^3) and BA (1.4 g/cm^3) were provided by suppliers.

The porosity (P) of the samples was determined using a density method as defined in the equation 2 (39).

$$P=(1-\frac{\boldsymbol{\rho_{app}}}{\boldsymbol{\rho_s}}) \times \mathbf{100}\% \qquad \text{(eq.2)}$$

The thermal conductivity of aerogels were measured using a Hot Disk equipment (TPS 2500S, Sweden) based on ISO 22007-2.2.

Compression tests were performed on a Hongda (China) universal testing machine using a load cell of 5 kN according to ISO 604. The crosshead rate and maximum strain were set to 2 mm/min and 70%, respectively. Five replicas of each sample were used.
Thermogravimetric analysis (TGA) was carried out on a Netzsch STA449F3 equipment (Germany) to study the thermal stability of aerogels. The tests were conducted at a nitrogen atmosphere at a heating rising ramp of 10 °C/min from 30 ^{o}C to 800 ^{o}C.
The limiting oxygen index (LOI) values were determined using an oxygen index meter (ATSFAAR 2008600, Italy) on the basis of ASTM D2863-2009. The dimensions of tested samples were 120x10x10 mm^3.
The vertical burning evaluation (UL-94) was performed on a HVUL2 instrument (Atalas, USA) following GT/T 8333-2008. The size of all samples used for testing was 125 x 10 x 10 mm^3.
The combustion behaviors of the composite aerogels were analyzed using a cone calorimeter (CC-1-X, Govmark, US) following ISO 5660 procedure. Square samples (100 x 100mm^2) with a thickness of 10mm were mounted in a steel support and exposed to an external heat flux of 50 kW/m^2.

3. Results and Discussion

3.1. Rheological Properties

The viscosities and shear stress of precursors for preparing aerogels were measured and results are displayed in Figure 1. The precursors showed a pseudo-plastic and a shear-thinning behavior. The zero-shear viscosity of precursors increased with the increase of BA content up to 0.75%. Interaction between free borate and hydroxyl groups on CNFs occured immediately when BA was added. This generated a network structure. However, a further increase in the BA content to 1.05% would lead to charge repulsion between free borate ions increased (40, 41), reducing the viscosities of precursors. MF resin loading further decreased the viscosities and shear stress because the existence of MF latex broke the molecular interaction between CNFs. Rheological properties of precursors play an important role in determining the pore structures of aerogels and their corresponding properties.

Figure 2. Rheologic properties of suspensions for preparing aerogels. (a) viscosity vs shear rate and (b) shear stress vs shear rate.

3.2. FTIR Spectroscopy Analysis

The FTIR spectra obtained from the aerogels are shown in Figure 3a. In regard to the control sample (C1.5M0.17), the characteristic band placed at 517 cm^{-1} was associated with the stretching vibration of clay's Al-O groups (42). The other characteristic band located at 1019 cm^{-1} was associated with asymmetry stretching of COC bonds that bridging the glucose units of cellulose. Peaks located at 3346 and 1587 cm^{-1} corresponded to OH stretching and OH bending, respectively (43). BA modified CNF aerogels displayed a new band at 1195 cm^{-1} attributed to the B-O groups formed due to the dehydration reaction of CNF and BA (44). With the addition of MF resins, a new band appeared at 1566 cm^{-1} that was assigned to the 1, 3, 5-s-triazing ring mode of melamine (45). Moreover, the reflection peak of OH (3346 cm^{-1}) shifted to 3206 cm^{-1}, suggesting that bonded water replaced free H_2O molecules. This was attributed to the reduction of hydroxyl groups on the CNFs after cross-linking reaction (43).

Figure 3. (a) FTIR spectra of CNF/MMT aerogels and cross-linked composite aerogels; Proposed scheme of (b) XPS spectra of sample C1.5M0.17 and C1.5M0.17B0.45.

3.3. XPS Spectra and Analysis

The XPS spectra of unmodified and BA crosslimked CNF/MMT aerogel (C1.5M0.17B0.45) are shown in Figure 3b. Regarding the unmidified sample, peaks at 286.1, 532.1, 102.3, 119 and 1071.1 eV contributed to C 1s, O 1s, Si 2p, Al 2s and Na 1s (46,47). After BA crosslinking, a new peak appearred at 192.3, which was associated with B 1s (48). The highest C atomic percentage was 50.6% in unmidified sample, whereas the C atomic percentage decreased to 43.8% when BA was introdeced. On the contract, B atomic concentration on the surface increased to 3.2%. Tiny amounts of B atoms (0.4%) in C1.5M0.17 was thought to be contamination on the surface.

High-resolution scan XPS spectra of C 1s, O 1s, and B 1s are shown in Figure 4. The C 1s spectra were divided into three subpeaks corresponding to different types of C-O bonds. The uncrosslinked CNF/MMT aerogels displayed strong peaks at 284.6 and 286.3 eV attributed to C-C and C-OH or O-C-O bonds, respectively. Another shoulder peaks at 287.9 attributed to -COOH (46).

The O 1s spectra of C1.5M0.15 showed a strong peak at 532.1 eV corresponded to C-OH bonds. The bands shifted to 531.9 eV could be assigned to C-O-B groups. The binding energie at 192.3 eV was assigned to B-O-C groups when boric acid was added (48). The XPS spetra analysis indicated that crosslinking between BA and nanocellulose occurred through an esterification reaction.

Figure 4. XPS spectra of unmodified and BA crosslinked aerogel (C1.5M0.15 and C1.5M0.15B0.45): high-resolution scans of (a) C 1s, (b) O 1s, and (c) B 1s.

3.4. Morphologies

CNF/MMT aerogels exhibited a typical lamellar structure as seen in Figure 5a. Solid impurities were reoriented by the growing ice front upon suspension freezing, ultimately forming the “house of cards” structure (49). The cell walls of foam-like aerogels were composed of clay nanoplatelets and entangled nanofibers. When a low content of BA (<0.5%) was added to the precursors, BA immediately cross-linked CNFs through a hydration or esterification reaction. The viscosity of precursor suspensions increased, generating higher resistance to the ice crystal growth (50). The corresponding aerogels maintained the lamellar structure but had compact cell-walls (Figure 5b & 5c). Further increase of BA quantity brought in a rough facture surface (Figure 5d). This was due to the fact that the ice front growth was affected by the increased fluid viscosity and secondary crystallization occurred. However, there was no a significant change on the aerogels’ microstructure when BA content was increased to 1.05% (Figure 5e) resulting from the reduced viscosity of the precursor suspension. This indicated that a BA level of 0.75% was the optimum concentration.

Figure 5. SEM micrographs of B/N FRAs modified CNF/MMT composite aerogels. (a) C1.5M0.17; (b) C1.5M0.17B0.15; (c) C1.5M0.17B0.45; (d) C1.5M0.17B0.75; (e) C1.5M0.17B1.05; (f) C1.5M0.17MF1.5B0.15; (g) C1.5M0.17MF1.5B0.45; (h) C1.5M0.17MF1.5B0.75; (i) C1.5M0.17MF1.5B1.05.

MF cross-linked CNF/MMT/BA aerogels showed more compact cell-walls, as seen in Figure 5f & 5g. This was attributed to the higher solids content of these compositions. Moreover, higher quantities of connecting struts composed by polymeric phase were observed. This was caused by the cross-linking of CNF and MF as well as the self-polymerization of MF resins (51). As the fraction of BA increased in CNF/MMT/MF/BA composite aerogels, oriented layers with tortuous holes were generated due to the increase of viscosity of corresponding precursor suspension (Figure 5h). Further increase of BA content to 1.05% did not significantly affect the structure of aerogels (Figure 5i). These structural features are consistent with the observed differences in compressive mechanical properties as discussed in following.

3.5. Compressive Properties

Compressive stress-strain curves of aerogels are shown in Figure 6a. All samples displayed typical elastic-plastic foam behavior. The apparent densities, compressive moduli (E), compressive stress at 70% of strain ($\sigma_{70\%}$) and specific moduli (Es) of composite aerogels are displayed in Figure 6.

The apparent densities of aerogels should increase with higher solid contents. However, when a low quantity of BA (<0.75%) was added, there was no significant change in the densities of cross-linked aerogels. This was due to the fact that inorganic BA loading reduced the shrinkage of CNF based aerogels, which resulted in a higher volume compared to uncross-linked ones. Regarding to the compressive properties, E and $\sigma_{70\%}$ increased by 84% and 60% respectively when the BA fraction reached 0.75%. Moreover, the specific modulus increased from 11.2 MPa to 18.1 MPa. These improvements in mechanical properties were due to the compact hydrogen bonds in BA cross-linked aerogels (50). However, further increase of BA amount in aerogel (1.05%) decreased the E and E_S values. One possible reason was that an excess BA content lowered the pH, limiting the

interfacial interaction between CNFs and clay (52). The other factor was the increased charge repulsion between free borate ions reduced the interaction between CNFs and BA as aforementioned.

The introduction of 1.5% of MF to C1.5M0.17B0.15 did not significantly change the compressive moduli. When BA was in low concentration in precursors, it first interacted with MF, retarding the cross-linking between CNFs and FRAs. With the BA's quantity increased in these compositions, dual cross-linking networks of CNFs-MF and CNFs-BA were formed, as seen in Figure 5f & 5g. As a result, E and $\sigma_{70\%}$ increased with the increase of BA content in CNF/MMT/MF/BA composite aerogels. When the BA content reached 0.75%, the corresponding aerogel had a modulus of 840 kPa and a maximum stress of 205.8 kPa. Nevertheless, a similar phenomenon occurred when the BA content was over 0.75%. The mechanical properties were reduced because the excessive BA interfered the bonding between CNFs and clay. In this case however, MF successfully cross-linked with CNF, C1.5M0.17MF1.5B1.05 and had much higher mechanical properties as compared to C1.5M0.17B1.05.

Figure 6. Compressive behavior of prepared aerogels: (a) Compressive curves of B/N FRA modified aerogels; (b) apparent densities, (c) compressive moduli, (d) compressive stress at 70% strain and (e) specific moduli of FRA modified aerogels versus BA content.

The CNF based aerogels in present work had a higher Young's moduli than those of diisocyanate crosslinked CNF aerogels (53). However, they showed inferior mechanical properties than those made with CNFs blended with a hydrophilic polymer (54). A reinforced cell-wall structure was formed in aerogels by encapsulating CNFs with polymers, making the foam-like materials withdraw higher load when they underwent bending.

3.6. Thermal Conductivity

The porosity and thermal conductivity (λ) were measured and the results are included in Table 1. Generally, a higher apparent density resulted in a lower porosity and therefore increased the thermal conductivity of aerogels. It was attributed to the thickening of pore walls leading to the higher conduction in solid

phase (55). However, in this work, the thermal conductivity of aerogels decreased as the reduction of their porosities. This was possible because BA crosslinking changed the vertical aligned structure of aerogels into a disrupted one, consuming more energy by reflection and scattering when the heat went through aerogels (56). The introduction of MF to CNF/MMT/BA composite aerogels further decreased the thermal conductivity. The MF modified composite aerogels had a thermal conductivity as low as 0.03 W/mK. This was ascribed to the fact that MF cross-linking and MF self-polymerization generated smaller pores as shown in SEM observation.

3.7. Thermal Stability

TGA weight loss and corresponding derivative thermogravimetric (DTG) curves of aerogels are shown in Figure 7. The relevant parameters, including the onset decomposition temperature ($T_{d5\%}$), maximum decomposition temperature (T_{dmax}), maximum mass decomposition rate (dW/dT_{max}) and residue amount (W_R) are summarized in Table 2. $T_{d2\%}$ was defined as the temperature at which 2% weight beyond total loss of moisture occurred after 150 °C.

Figure 7. TGA (a) and DTG (b) curves of B/N FRAs modified CNFs based aerogels.

The increase of T_{dmax} and a significant decrease of dW/dT_{max} after the BA cross-linking demonstrated an improvement of thermal stability of aerogels. BA cross-linking also increased the residue, implying more char structure remained under the catalysis of boron (50). The blank sample showed an initial decomposition temperature ($T_{d2\%}$) of 257 ^{o}C, which was due to the breaking of CNFs' molecular chains. When 0.15% of BA was incorporated, $T_{d2\%}$ of cross-linked aerogel increased to 274 ^{o}C. It suggested that CNF underwent a thermally induced esterification/cross-linking process, retarding the pyrolysis of CNFs' molecular backbones (57). However, further increase in BA content decreased the initial decomposition temperature. The T_{dmax} also began to decline when the BA content was higher than 0.45%. This was possibly because the thermal conductivity of

aerogels increased as well at high BA contents. When the BA increased to 1.05%, $T_{d2\%}$ was even lower than the one of control sample. This effect was caused by an excess of BA that did not take part in the esterification reaction decomposed at a lower temperature (<200 ^{o}C). Moreover, the residue content did not show significant change. An excess BA lowered the pH, prior reactivity of borate anion toward carboxylic groups on the nanocellulose backbone occurred (36).

A similar tendency on thermal stability was observed when 1.5% of MF resin was added to CNF/MMT aerogels cross-linked with different amounts of BA. Free floating MF that was detected by FT-IR analysis in the aerogels decomposed at ~180 ^{o}C (58). This caused a lower $T_{2\%}$ was observed among the aerogels treated with MF. The pyrolysis of MF resins released NH_3 (59), diminishing the decomposition rate (dW/dT_{max}). However, organic MF had less contribution on char formation, causing the reduction of residue amounts compared with samples free of MF.

3.8. Flammability

Limiting oxygen index (LOI) and UL-94 tests were conducted to investigate the effect of BA and MF cross-linking on the flammability of the CNF/MMT aerogels. The corresponding results are included in Table 3. Sample C1.5M0.17 had a low LOI value of 17.8% and showed no UL-94 rating. In comparison to the pure CNF aerogels from our previous work (LOI=17.1%) (51), the addition of MMT did not significantly change the LOI value. With the addition of BA, the LOI values increased proportionaly to the BA amount. Especially when the BA fraction exceeded 0.75%, the LOI values of aerogels were higher than 40 and UL-94 rating reached V-0, which was characteristic of high flame retardant materials. This was due to the dehydration assisted by BA cross-linking which formed a thermally insulating, glassy protective carbonized layer in the condensed phase (36), restricting the oxygen and heat propagation in the materials. It was also observed that the aerogel with this composition showed a self-extinguishing property and merely shrank a little after 60 s of ignition by an alcohol burner, as shown in Figure 8b.

Figure 8. Photos of C1.5M0.17 (a) and C1.5M0.17B0.75 (b) samples after different time of ignition by an alcohol burner.

The LOI values also increased with MF cross-linking. 1.5 % MF addition increased the LOI value of C1.5M0.17B0.15 to 33% and improved the UL-94 level to V-1. This was because the decomposition of MF which released NH_3, diluted the fuel gas and hindered the spread of flame (59). BA interacted with MF during burning generated more compact carbonaceous layers and constructed a gas-condensed flame retardant effect. When 1.5% of MF was loaded, the LOI value of C1.5M0.17B1.05 significantly increased from 58.2% to ~85%. This fact suggested a synergistic effect between BA and MF on the flame retardant properties of CNF/MMT aerogels. The LOI value of the B/N FRA modified CNF based aerogels was much higher than those reported for flame retardant polymer-based aerogels or foams, such as CNF/MoS_2 aerogel (LOI=34.7%) (32), PVA/MF aerogels (LOI=36.5%) (59), and PVA/MMT/APP (LOI=42%) (60).

Figure 9. (a) Heat release rate of prepared aerogels as a function of burning time; (b) and (c) Char photos of sample C1.5M0.17 and C1.5M0.17B0.75, respectively.

The combustion of representative aerogels was also studied through cone calorimetry tests which could mimic the combustion behavior of a material in a real fire scenario. The heat release rate as a function of burning time is shown in Figure 9a. Corresponding parameters including peak of heat release rate (PHRR), time to PHRR (TTPHRR), total heat release (THR), fire growth rate (FGR) and residue amount (W_R) are listed in Table 4.

C1.5M0.17 displayed a sharp burning peak at 50 s with a PHRR of 24.1 kW/m^2. The BA cross-linking lowered the fire risk indexes of PHRR and THR. Especially, when the BA content increased to 0.75%, the FGR reduced to 0.21 W/s and the char residue amount reached 39%. The comparison of the char created after cone calorimetry with that of control samples is shown in Figure 9b & 9c. A more compact char was obtained. Samples containing 1.05% of BA were not selected to be tested due to their no flammability.

The addition of 1.5% MF further decreased the PHRR, THR and FGR, indicating a synergistic effect between BA and MF on the flame retardant properties of CNF/MMT aerogels. However, there was no significant change on the residue content. This was because MF mainly acted in the gas-phase releasing NH_3 during combustion.

4. Conclusions

In this work, low-flammability CNF/MMT aerogels with improved mechanical properties via cross-linking with B/N containing flame retardant agents were successfully prepared. The CNF/MMT aerogel had a porous lamellar structure with cell walls composed of CNFs and clay. Undergoing the cross-linking of BA, the aerogels showed thicker layers and narrower interspacing due to the increased viscosities of precursor suspensions. MF cross-linking led to the formation of polymeric struts which connected the layers. The optimum BA fraction for improving the compressive moduli and compressive stress of aerogels was found to be 0.75%. The onset decomposition temperature could be increased by nearly 40 ^{o}C after simple BA cross-linking. The LOI value of the corresponding aerogels also increased and the UL-94 grade reached V-0. On this basis, the addition of 1.5% MF further improved the mechanical properties of the composite aerogels. In addition, the flammability of aerogels was greatly decreased due to the synergistic flame retardant effect between BA and MF. It was worth noting that the highest LOI value of the prepared sample in this work was 85%. The prepared CNF composite aerogels had good mechanical properties as well as low thermal conductivity and low flammability, opening the door to a wide range of potential applications.

Acknowledgments: This work was financially supported by Science & Technology Development Fund of Tianjin Education Commission for Higher Education (2017KJ069).

Conflicts of Interest: The authors declare no conflict of interest.

References

1. Hüsing N, Schubert U. Aerogels-airy materials: chemistry, structure, and properties. *Angewandte Chemie International Edition*. 1998;**37**(1−2):22-45.

2. Kistler S. Coherent Expanded Aerogels and Jellies. *Nature*. 1931;**127**(3211):741.

3. Kistler S. Coherent expanded-aerogels. *The Journal of Physical Chemistry*. 1932;**36**(1):52-64.

4. Bendahou D, Bendahou A, Seantier B, Grohens Y, Kaddami H. Nano-fibrillated cellulose-zeolites based new hybrid composites aerogels with super thermal insulating properties. *Industrial Crops & Products*. 2015;**65**:374-382.

5. Moreno-Castilla C, Maldonado-Hódar FJ. Carbon aerogels for catalysis applications: An overview. *Carbon*. 2005;**43**(3):455-465.

6. Maleki H. Recent advances in aerogels for environmental remediation applications: A review. *Chemical Engineering Journal*. 2016;**300**:98-118.

7. Stergar J, Maver U. Review of aerogel-based materials in biomedical applications. *Journal of Sol-Gel Science and Technology*. 2016;**77**(3):738-752.

8. Zhang Y, Zuo L, Zhang L, Huang Y, Lu H, Fan W, et al. Cotton wool derived carbon fiber aerogel supported few-layered $MoSe_2$ nanosheets as efficient electrocatalysts for hydrogen evolution. *ACS Applied Materials & Interfaces*. 2016;**8**(11):7077-85.

9. Xu X, Zhou J, Nagaraju DH, Jiang L, Marinov VR, Lubineau G, et al. Flexible, Highly Graphitized Carbon Aerogels Based on Bacterial Cellulose/Lignin: Catalyst−Free Synthesis and its Application in Energy Storage Devices. *Advanced Functional Materials*. 2015;**25**(21):3193-3202.

10. Gawryla MD, Nezamzadeh M, Schiraldi DA. Foam-like materials produced from abundant natural resources. *Green Chemistry*. 2008;**10**:1078-1081.

11. Chen HB, Wang YZ, Sánchez-Soto M, Schiraldi DA. Low flammability, foam-like materials based on ammonium alginate and sodium montmorillonite clay. *Polymer*. 2012;**53**(25):5825-5831.

12. Chen HB, Chiou BS, Wang YZ, Schiraldi DA. Biodegradable pectin/clay aerogels. *ACS Applied Materials & Interfaces*. 2013;**5**(5):1715-1721.

13. Rudaz C, Courson R, Bonnet L, Calas-Etienne S, Sallée H, Budtova T. Aeropectin: fully biomass-based mechanically strong and thermal superinsulating aerogel. *Biomacromolecules*. 2014;**15**(6):2188-2195.

14. Wang L, Schiraldi DA, Sánchez-Soto M. Foamlike Xanthan Gum/Clay Aerogel Composites and Tailoring Properties by Blending with Agar. *Industrial & Engineering Chemistry Research*. 2014;**53**(18):7680–7687.

15. Wang L, Sánchez−Soto M, Abt T, Maspoch ML, Santana OO. Microwave-crosslinked bio-based starch/clay aerogels. *Polymer International*. 2016;**65**(8):899-904.

16. Guhados G, Wan W, Hutter JL. Measurement of the elastic modulus of single bacterial cellulose fibers using atomic force microscopy. *Langmuir*. 2005;**21**(14):6642-6646.

17. Hsieh YC, Yano H, Nogi M, Eichhorn SJ. An estimation of the Young's modulus of bacterial cellulose filaments. *Cellulose*. 2008;**15**(4):507-513.

18. Pääkkö M, Vapaavuori J, Silvennoinen R, Kosonen H, Ankerfors M, Lindström T, et al. Long and entangled native cellulose I nanofibers allow flexible aerogels and hierarchically porous templates for functionalities. *Soft Matter*. 2008;**4**(12):2492-2499.

19. Sehaqui H, Salajkova M, Zhou Q, Berglund LA. Mechanical performance tailoring of tough ultra-high porosity foams prepared from cellulose I nanofiber suspensions. *Soft Matter*. 2010;**6**(8):1824-1832.

20. Svagan AJ, Samir MASA, Berglund LA. Biomimetic Foams of High Mechanical Performance Based on Nanostructured Cell Walls Reinforced by Native Cellulose Nanofibrils. *Advanced Materials*. 2010;**20**(7):1263-1269.

21. Svagan AJ, Berglund LA, Jensen P. Cellulose nanocomposite biopolymer foam--hierarchical structure effects on energy absorption. *ACS Applied Materials & Interfaces*. 2011;**3**(5):1411-1417.

22. Liu D, Ma Z, Wang Z, Tian H, Gu M. Biodegradable poly(vinyl alcohol) foams supported by cellulose nanofibrils: processing, structure, and properties. *Langmuir* 2014;**30**(31):9544-9550.

23. Chen B, Zheng Q, Zhu J, Li J, Cai Z, Chen L, et al. Mechanically strong fully biobased anisotropic cellulose aerogels. *RSC Advances*. 2016;**6**(99):96518-9626.

24. Heidarian P, Behzad T, Sadeghi M. Investigation of cross-linked PVA/starch biocomposites reinforced by cellulose nanofibrils isolated from aspen wood sawdust. *Cellulose*. 2017;**24**(8):3323-3339.

25. Verdolotti L, Stanzione M, Khlebnikov O, Silant'ev V, Postnova I, Lavorgna M, et al. Dimensionally Stable Cellulose Aerogel Strengthened by Polyurethane Synthesized In Situ. *Macromolecular Chemistry and Physics*. 2019;**220**(1):1800372. https://doi.org/10.1002/macp.201800372.

26. Kim CH, Youn HJ, Lee HL. Preparation of cross-linked cellulose nanofibril aerogel with water absorbency and shape recovery. *Cellulose*. 2015;**22**(6):3715-3724.

27. Jiang F, Hsieh YL. Cellulose Nanofibril Aerogels: Synergistic Improvement of Hydrophobicity, Strength, and Thermal Stability via Cross-Linking with Diisocyanate. *ACS Applied Materials & Interfaces*. 2017;**9**(3):2825-2834.

28. Han Y, Zhang X, Wu X, Lu C. Flame Retardant, Heat Insulating Cellulose Aerogels from Waste Cotton Fabrics by in Situ Formation of Magnesium Hydroxide Nanoparticles in Cellulose Gel Nanostructures. *ACS Sustainable Chemistry & Engineering*. 2015;**3**(8):1853-1859.

29. Yuan B, Zhang J, Yu J, Song R, Mi Q, He J, et al. Transparent and flame retardant cellulose/aluminum hydroxide nanocomposite aerogels. *Science China Chemistry*. 2016;**59**(10):1335-1341.

30. Yuan B, Zhang JM, Mi Q, Yu J, Song R, Zhang J. Transparent Cellulose-silica composite aerogels with excellent flame retardancy via in situ sol-gel process. *ACS Sustainable Chemistry & Engineering*. 2017;**5**:1117-1123.

31. Wicklein B, Kocjan A, Salazar-Alvarez G, Carosio F, Camino G, Antonietti M, et al. Thermally insulating and fire-retardant lightweight anisotropic foams based on nanocellulose and graphene oxide. *Nat Nanotechnol*. 2015;**10**(3):277-283.

32. Yang L, Mukhopadhyay A, Jiao YC, Yong Q, Chen L, Xing YJ, et al. Ultralight, highly thermally insulating and fire resistant aerogel by encapsulating cellulose nanofibers with two-dimensional MoS_2. *Nanoscale*. 2017;**9**(32):11452-11462.

33. Koklukaya O, Carosio F, Wagberg L. Superior Flame-Resistant Cellulose Nanofibril Aerogels Modified with Hybrid Layer-by-Layer Coatings. *ACS Applied Materials & Interfaces*. 2017;**9**(34):29082-29092.

34. Wang L, Sanchez-Soto M. Green bio-based aerogels prepared from recycled cellulose fiber suspensions. *RSC Advances*. 2015;**5**(40):31384-31391.

35. Ghanadpour M, Wicklein B, Carosio F, Wagberg L. All-natural and highly flame-resistant freeze-cast foams based on phosphorylated cellulose nanofibrils. *Nanoscale*. 2018;**10**(8):4085-4095.

36. Wicklein B, Kocjan D, Carosio F, Camino G, Bergström L. Tuning the Nanocellulose-Borate Interaction To Achieve Highly Flame Retardant Hybrid Materials. *Chemistry of Materials*. 2016;**28**(7):1985-1989.

37. Guo L, Chen Z, Lyu S, Fu F, Wang S. Highly flexible cross-linked cellulose nanofibril sponge-like aerogels with improved mechanical property and enhanced flame retardancy. *Carbohydrate Polymers*. 2018;**179**:333-340.

38. Laoutid F, Bonnaud L, Alexandre M, Lopez-Cuesta JM, Dubois P. New prospects in flame retardant polymer materials: From fundamentals to nanocomposites. *Materials Science & Engineering R-Reports*. 2009;**63**(3):100-125.

39. Gibson LJ, Ashby MF. Cellular solids: structure and properties. 2nd ed: Cambridge university press; 1999.

40. Pezron E, Ricard A, Lafuma F, Audebert R. Reversible gel formation induced by ion complexation. 1. Borax-galactomannan interactions. *Macromolecules*. 1988;**21**(4):1126-1131.

41. Kurokawa H, Shibayama M, Ishimaru T, Nomura S, Wu WL. Phase behaviour and sol-gel transition of poly(vinyl alcohol)-borate complex in aqueous solution. *Polymer*. 1992;**33**(10):2182-2188.

42. Chen D, Xu Y, Zang Y, Su S. Effect of polymerically-modified clay structure on the morphology and properties of UV-cured polyurethane acrylate/clay nanocomposites. *Polymers for Advanced Technologies*. 2011;**22**(12):1919-1924..

43. Socrates G, Socrates G. Infrared and Raman characteristic group frequencies: tables and charts. Third ed: Wiley Chichester; 2001. PP 329.

44. Spoljaric S, Salminen A, Luong ND, Seppälä J. Stable, self-healing hydrogels from nanofibrillated cellulose, poly(vinyl alcohol) and borax via reversible crosslinking. *European Polymer Journal*. 2014;**56**(7):105-117.

45. Wu Y, Li Y, Qin L, Yang F, Wu D. Monodispersed or narrow-dispersed melamine-formaldehyde resin polymer colloidal spheres: preparation, size-control, modification, bioconjugation and particle formation mechanism. *Journal of Materials Chemistry B*. 2013;**1**(2):204-212.

46. Espino-Pérez E, Domenek S, Belgacem N, Sillard C, Bras J. Green Process for Chemical Functionalization of Nanocellulose with Carboxylic Acids. *Biomacromolecules*. 2014;**15**:4551-4560.

47. Senarathna KGC, Randiligama HMSP, Rajapakse RMG. Preparation, characterization and oxygen reduction catalytic activities of nanocomposites of Co(II)/montmorillonite containing polypyrrole, polyaniline or poly(ethylenedioxythiophene). *RSC Advances*. 2016;**6**:112853-112863.

48. Lai CL, Chen JT, Fu YJ, Liu WR, Zhong YR, Huang SH, et al. Bio-inspired cross-linking with borate for enhancing gas-barrier properties of poly(vinyl alcohol)/graphene oxide composite films. *Carbon*. 2015;**82**:513-522.

49. Bandi S, Bell M, Schiraldi DA. Temperature-responsive clay aerogel-polymer composites. *Macromolecules*. 2005;**38**(22):9216-9220.

50. Shang K, Ye DD, Kang AH, Wang YT, Liao W, Xu S, et al. Robust and fire retardant borate-crosslinked poly (vinyl alcohol)/montmorillonite aerogel via melt-crosslink. *Polymer*. 2017;**131**:111-119.

51. Wang L, Cui L, Sánchez-Soto M, Shou W, Xia Z, Liu Y. Highly Flame Retardant Melamine-Formaldehyde Cross-Linked Cellulose Nanofibrils/Sodium Montmorillonite Aerogels with Improved Mechanical Properties. *Macromolecular Materials and Engineering*. 2018:1800379. https://doi.org/10.1002/mame.201800379.

52. Gawryla MD, Liu L, Grunlan JC, Schiraldi DA. pH Tailoring Electrical and Mechanical Behavior of Polymer-Clay-Nanotube Aerogels. *Macromolecular Rapid Communications*. 2009;**30**(19):1669-1673.

53. Jiang F, Hsieh YL. Cellulose Nanofibril Aerogels: Synergistic Improvement of Hydrophobicity, Strength, and Thermal Stability via Cross-Linking with Diisocyanate. *ACS Applied Materials & Interfaces*. 2017;**9**:2825-2834.

54. Liu A, Medina L, Berglund LA. High-Strength Nanocomposite Aerogels of Ternary Composition: Poly(vinyl alcohol), Clay, and Cellulose Nanofibrils. *ACS Applied Materials & Interfaces*. 2017;**9**:6453-6461.

55. Koebel M. Aerogel-based thermal superinsulation: an overview. *Journal of Sol-Gel Science and Technology*. 2012;**63**(3):315-339.

56. Hostler SR, Abramson AR, Gawryla MD, Bandi SA, Schiraldi DA. Thermal conductivity of a clay-based aerogel. *International Journal of Heat and Mass Transfer*. 2009;**52**(3-4):665-669.

57. Visakh PM, Nazarenko OB, Amelkovich YA, Melnikova TV. Effect of zeolite and boric acid on epoxy-based composites. *Polymers for Advanced Technologies*. 2016;**27**(8):1098-1101.

58. Jiang Y, Zhou W, Jiang M, Liu P, Xu J. Flame retardant study of formalized polyvinyl alcohol fiber coated with melamine formaldehyde resins and the synergistic effect of copper ions. *Polymer Degradation & Stability*. 2017;**144**:331-343.

59. Shang K, Yang JC, Cao Z, Liao W, Wang YZ, Schiraldi DA. A novel polymer aerogel towards high dimensional stability, mechanical property and fire safety. *ACS Applied Materials & Interfaces*. 2017;**9**(27):22985-22993.

60. Wang YT, Liao SF, Shang K, Chen MJ, Huang JQ, Wang YZ, et al. Efficient Approach to Improving the Flame Retardancy of Poly(vinyl alcohol)/Clay Aerogels: Incorporating Piperazine-Modified Ammonium Polyphosphate. *ACS Applied Materials & Interfaces*. 2015;**7**(3):1780-1786.

Lists of figure caption

Figure 1. Scheme illustrating the procedure used to synthesize N/B FRAs modified CNF/MMT composite aerogels.

Figure 2. Rheologic properties of suspensions for preparing aerogels. (a) viscosity vs shear rate and (b) shear stress vs shear rate.

Figure 3. (a) FTIR spectra of CNF/MMT aerogels and cross-linked composite aerogels; Proposed scheme of (b) XPS spectra of sample C1.5M0.17 and C1.5M0.17B0.45.

Figure 4. XPS spectra of unmodified and BA crosslinked aerogel (C1.5M0.15 and C1.5M0.15B0.45): high-resolution scans of (a) C 1s, (b) O 1s, and (c) B 1s.

Figure 5. SEM micrographs of B/N FRAs modified CNF/MMT composite aerogels. (a) C1.5M0.17; (b) C1.5M0.17B0.15; (c) C1.5M0.17B0.45; (d) C1.5M0.17B0.75; (e) C1.5M0.17B1.05; (f) C1.5M0.17MF1.5B0.15; (g) C1.5M0.17MF1.5B0.45; (h) C1.5M0.17MF1.5B0.75; (i) C1.5M0.17MF1.5B1.05.

Figure 6. Compressive behavior of prepared aerogels: (a) Compressive curves of B/N FRA modified aerogels; (b) apparent densities, (c) compressive moduli, (d) compressive stress at 70% strain and (e) specific moduli of FRA modified aerogels versus BA content.

Figure 7. TGA (a) and DTG (b) curves of B/N FRAs modified CNFs based aerogels.

Figure 8. Photos of C1.5M0.17 (a) and C1.5M0.17B0.75 (b) samples after different time of ignition by an alcohol burner.

Figure 9. (a) Heat release rate of prepared aerogels as a function of burning time; (b) and (c) Char photos of sample C1.5M0.17 and C1.5M0.17B0.75, respectively.

Table 1. The porosity and thermal conductivity of prepared aerogels.

Samples	Porosity (%)	λ (W/mK)
C1.5M0.17	98.4	0.035±0.001
C1.5M0.17B0.15	98.5	0.035±0.001
C1.5M0.17B0.45	98.5	0.034±0.001
C1.5M0.17B0.75	98.2	0.033±0.001
C1.5M0.17B1.05	97.9	0.033±0.001
C1.5M0.17MF1.5B0.15	98.2	0.032±0.001
C1.5M0.17MF1.5B0.45	98.1	0.031±0.001
C1.5M0.17MF1.5B0.75	97.8	0.030±0.001
C1.5M0.17MF1.5B1.05	97.6	0.030±0.001

Table 2. TGA data of B/N FRAs modified CNF based aerogels.

Samples	$T_{d2\%}$ [°C]	T_{dmax} [°C]	dW/dT_{max} [%/°C]	W_R [%]
C1.5M0.17	257	286	7.59	32.2
C1.5M0.17B0.15	274	311	3.70	40.9
C1.5M0.17B0.45	257	325	3.42	48.3
C1.5M0.17B0.75	256	315	2.69	57.5
C1.5M0.17B1.05	252	311	2.55	55.8
C1.5M0.17MF1.5B0.15	220	309	3.20	37.2
C1.5M0.17MF1.5B0.45	220	310	3.15	42.3
C1.5M0.17MF1.5B0.75	235	300	2.40	53.1
C1.5M0.17MF1.5B1.05	214	299	2.36	53.1

Table 3. LOI measurements and UL-94 tests results of the prepared aerogels.

Samples	LOI (%)	UL-94
C1.5M0.17	17.8	NR
C1.5M0.17B0.15	20.7	NR
C1.5M0.17B0.45	25	NR
C1.5M0.17B0.75	42.7	V-0
C1.5M0.17B1.05	58.2	V-0
C1.5M0.17MF1.5B0.15	33	V-1
C1.5M0.17MF1.5B0.45	42.3	V-0
C1.5M0.17MF1.5B0.75	65.2	V-0
C1.5M0.17MF1.5B1.05	~85	V-0

Table 4. Combustive parameters of the prepared CNF based aerogels from cone calorimetry.

Samples	PHRR [kW/m^2]	TTPHRR [s]	THR [MJ/m^2]	FGR [W/s]	W_R [%]
C1.5M0.17	28.9±4.8	50	3.05±0.85	0.48	28±3.1
C1.5M0.17B0.15	27.8±5.1	80	2.93±0.76	0.28	29±2.9
C1.5M0.17B0.45	26.0±4.5	80	2.27±0.72	0.27	31±3.0
C1.5M0.17B0.75	19.4±3.7	80	1.70±0.81	0.21	39±2.8
C1.5M0.17MF1.5B0.15	21.7±4.2	90	2.69±0.91	0.19	23±3.5
C1.5M0.17MF1.5B0.45	18.6±4.8	125	1.97±0.85	0.11	35±2.7
C1.5M0.17MF1.5B0.75	12.3±3.9	135	1.51±0.54	0.06	45±3.3

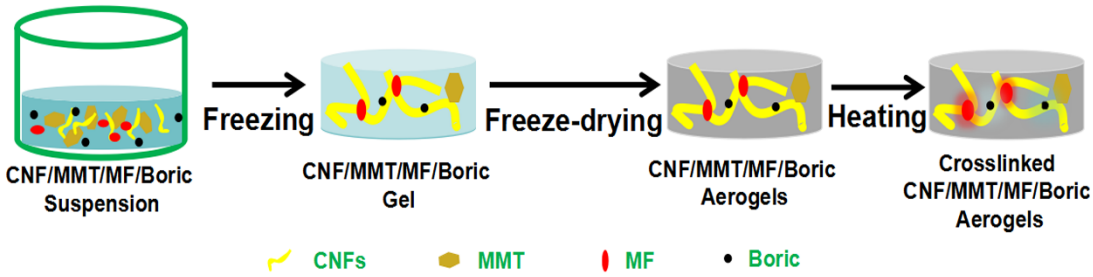

Figure 1. Scheme illustrating the procedure used to synthesize N/B FRAs modified CNF/MMT composite aerogels.

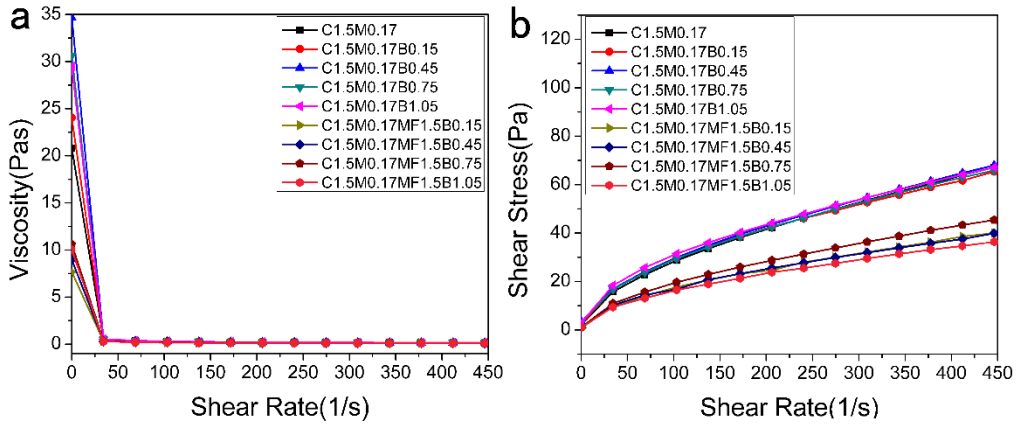

Figure 2. Rheologic properties of suspensions for preparing aerogels. (a) viscosity vs shear rate and (b) shear stress vs shear rate.

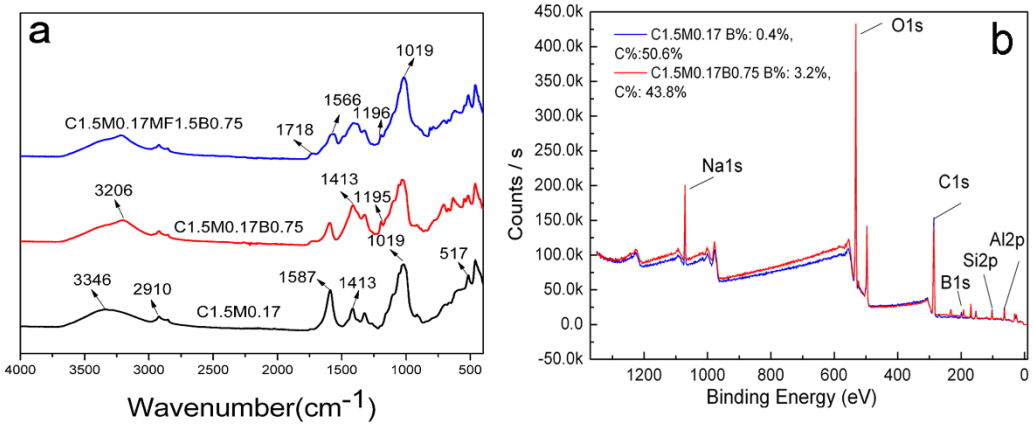

Figure 3. (a) FTIR spectra of CNF/MMT aerogels and cross-linked composite aerogels; Proposed scheme of (b) XPS spectra of sample C1.5M0.17 and C1.5M0.17B0.45.

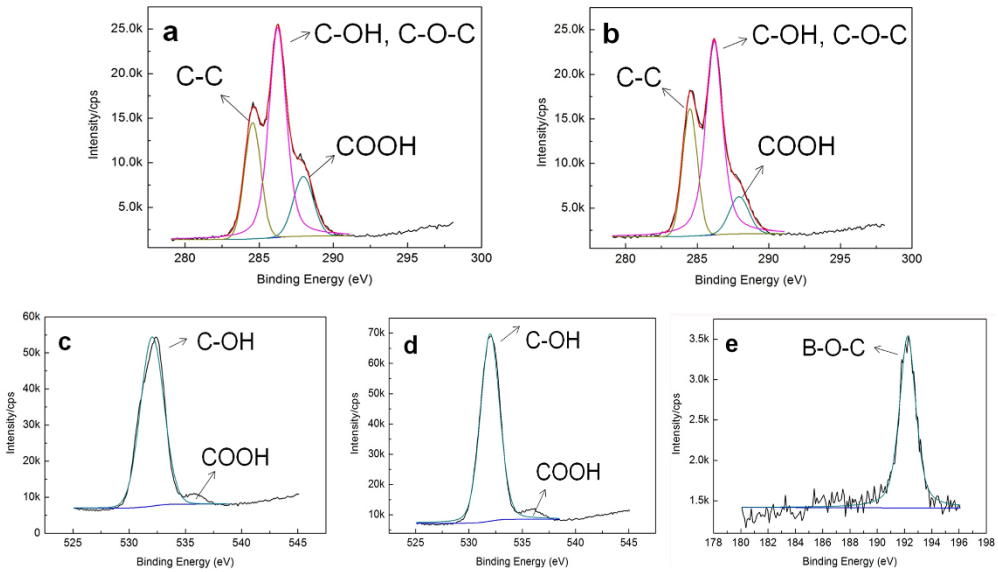

Figure 4. XPS spectra of unmodified and BA crosslinked aerogel (C1.5M0.15 and C1.5M0.15B0.45): high-resolution scans of (a) C 1s, (b) O 1s, and (c) B 1s.

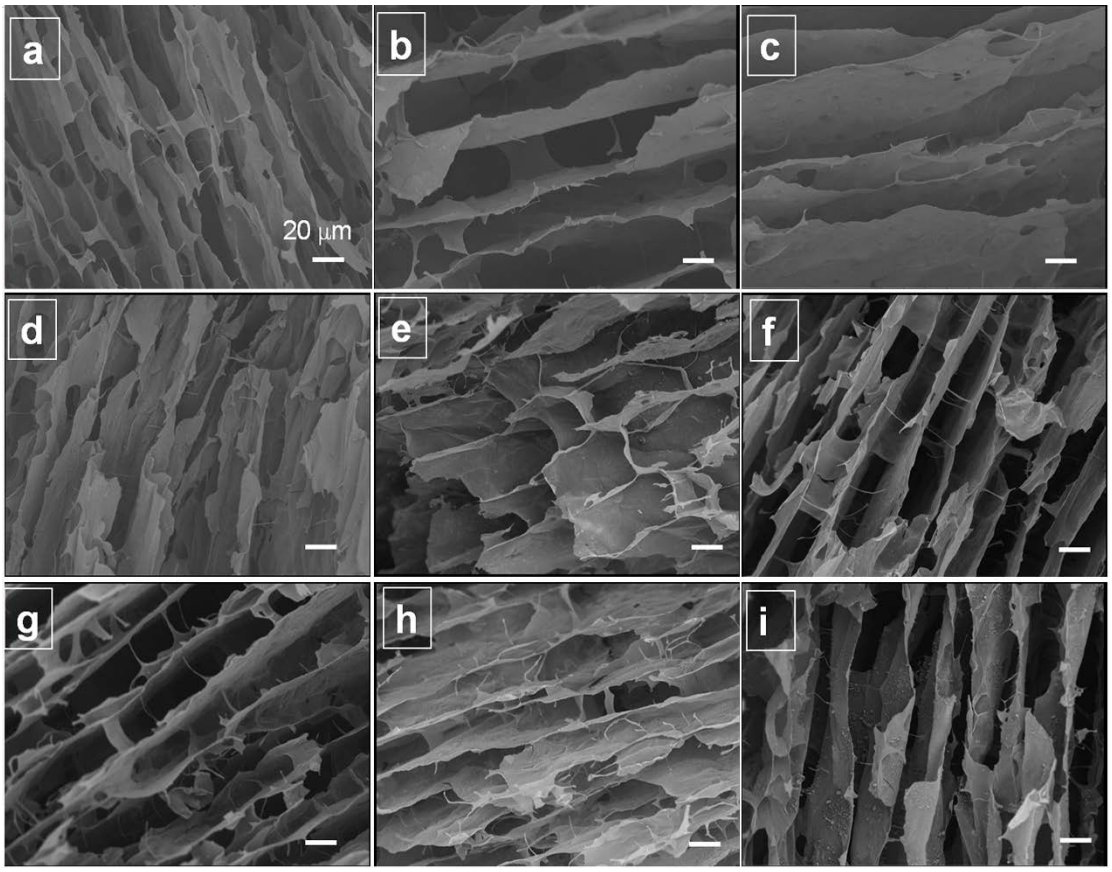

Figure 5. SEM micrographs of B/N FRAs modified CNF/MMT composite aerogels. (a) C1.5M0.17; (b) C1.5M0.17B0.15; (c) C1.5M0.17B0.45; (d) C1.5M0.17B0.75; (e) C1.5M0.17B1.05; (f) C1.5M0.17MF1.5B0.15; (g) C1.5M0.17MF1.5B0.45; (h) C1.5M0.17MF1.5B0.75; (i) C1.5M0.17MF1.5B1.05.

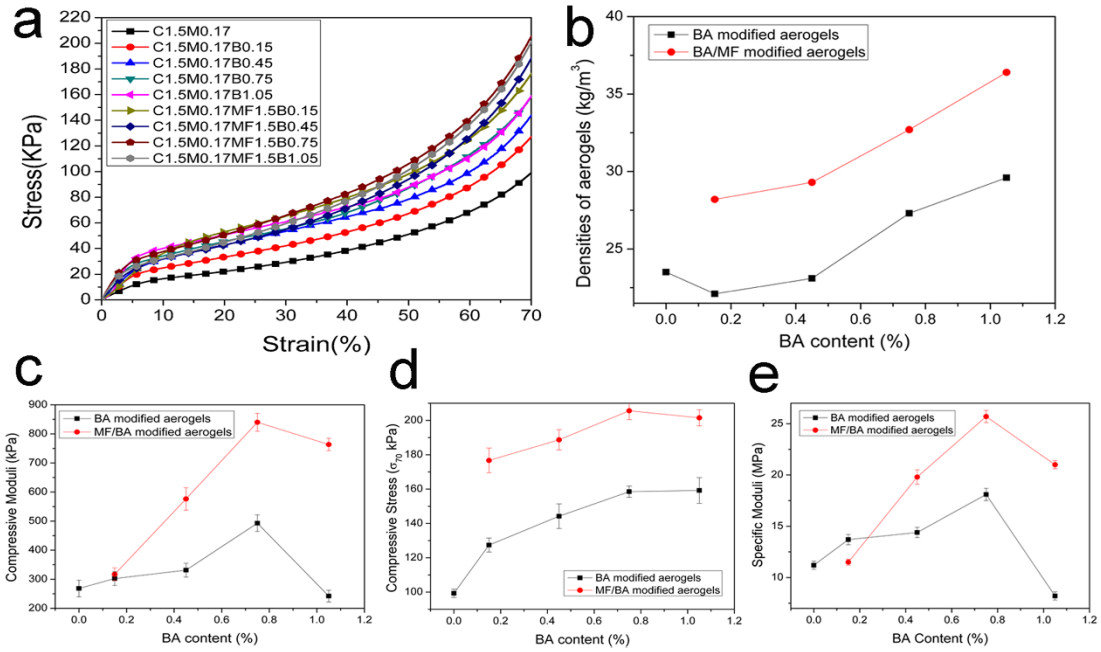

Figure 6. Compressive behavior of prepared aerogels: (a) Compressive curves of B/N FRA modified aerogels; (b) apparent densities, (c) compressive moduli, (d) compressive stress at 70% strain and (e) specific moduli of FRA modified aerogels versus BA content.

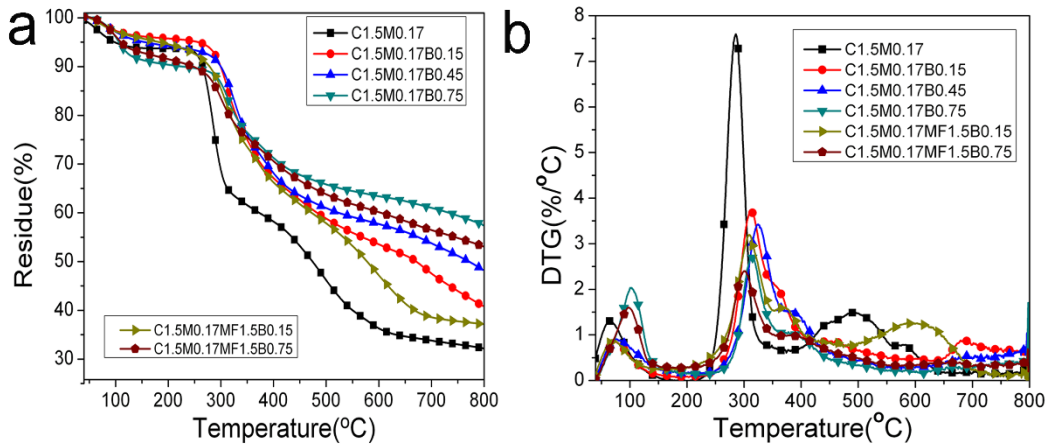

Figure 7. TGA (a) and DTG (b) curves of B/N FRAs modified CNFs based aerogels.

Figure 8. Photos of C1.5M0.17 (a) and C1.5M0.17B0.75 (b) samples after different time of ignition by an alcohol burner.

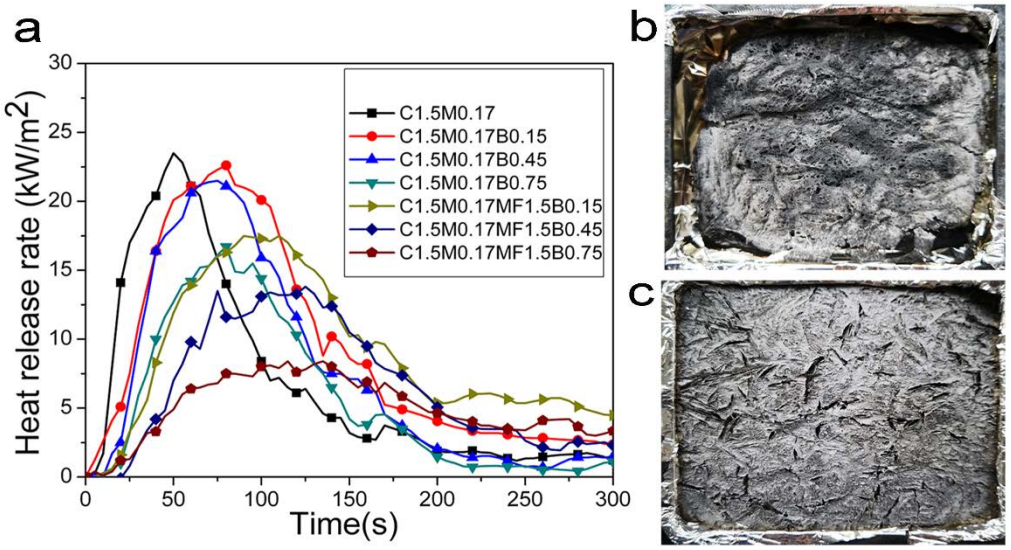

Figure 9. (a) Heat release rate of prepared aerogels as a function of burning time; (b) and (c) Char photos of sample C1.5M0.17 and C1.5M0.17B0.75, respectively.